

Theoretical Determination of the Redox Potentials of NRH:Quinone Oxidoreductase 2 Using Quantum Mechanical/Molecular Mechanical Simulations

James C. Rauschnot, Jr., Chee Yang, Vang Yang, and Sudeep Bhattacharyya*

Department of Chemistry, University of Wisconsin-Eau Claire, 105 Garfield Avenue, Eau Claire, Wisconsin 54702

Received: February 28, 2009; Revised Manuscript Received: April 27, 2009

NRH:quinone oxidoreductase 2 (NQO2) is a flavoenzyme that catalyzes a one-step two-electron reduction of quinones. During this enzyme catalysis, the 7,8-dimethyl isoalloxazine (flavin) ring of the enzyme-bound cofactor, flavin adenine dinucleotide (FAD), shuttles between reduced and oxidized states as the enzyme passes through multiple cycles of binding/release of alternate substrates. These redox changes in NQO2, however, lead to unequal charge separation between the flavin ring and the active site, which must be stabilized by reorganization of the surrounding protein matrix. In this study, we have used a combined quantum mechanical/molecular mechanical method to simulate the electron and proton addition reactions of the flavin-bound NQO2. We have computed the redox potentials and pK_a 's of the enzyme-bound flavin. The present work demonstrates that upon reduction, the NQO2 active site stabilizes the flavin anionic hydroquinone state. Simulation data has also allowed quantitative estimation of the electrostatic contributions of active site residues. Their significance in oscillatory redox transition of this flavoenzyme is discussed.

1. Introduction

Dihyronicotinamide riboside (NRH):quinone oxidoreductase 2 (NQO2) and its close analog, NADPH:quinone oxidoreductase 1 (NQO1) belong to a group of cytosolic enzymes, known as quinone reductases (QR). Xenobiotics and antioxidants induce the expression of these enzymes,¹ whose normal intracellular activity involves a catalytic single-step reduction of quinones to hydroquinones, through use of an organic cofactor, flavin adenosine dinucleotide (FAD).^{2,3} Of absolute significance is the redox chemistry of QR, which is associated with two beneficial consequences: (i) promotion of natural defense mechanisms that combat against oxidative and chemical stresses by protecting humoral B-cells^{3–5} from harmful semiquinones and (ii) activation of anticancer chemotherapeutic agents^{3,5,6} or prodrugs through in vivo conversions to DNA–DNA cross-linkers.

Central to the prodrug activation and resistance to oxidative damages lies an interesting redox chemistry of the enzyme-bound cofactor. The enzyme catalysis of QR follows a classic one-site ping-pong mechanism.^{5,7,8} In the reductive half-cycle of NQO2, FAD is reduced by accepting a hydride from NRH. Following the release of nicotinamide riboside, the quinone then binds to the emptied enzyme pocket and accepts a hydride from the reduced flavin thereby completing the redox cycle. Successful completion of this reaction is key to the release of oxidative stress in cells because it competes with another biotransformation, the cytochrome P450 reductase-catalyzed one-electron conversion of the quinones. This parallel pathway yields highly unstable radical semiquinones, which subsequently reacts with molecular oxygen to produce highly reactive oxygen species (ROS).⁵ Therefore, the catalytic single-step reduction of quinones to hydroquinones by quinone reductases acts as a preventive mechanism against the ROS formation in cells.⁵

The catalytic reduction of FAD leads to an unfavorable charge separation that must be stabilized by the surrounding protein

matrix. The detail of this charge stabilization is experimentally inaccessible but extremely important for the binding of prodrugs or other quinones and their subsequent catalytic conversions.

The reduction of flavoenzymes typically involves coupled electron–proton transfers.^{9,10} In this work, we explored these proton-coupled reduction processes of the flavin-bound NQO2 using theoretical means. In particular, we used a combined quantum mechanical/molecular mechanical (QM/MM) method,¹¹ where the tricyclic flavin ring atoms were treated by higher level of computing protocol (SCC-DFTB, self-consistent-charge density functional tight-binding)^{12–14} while embedded in the classically treated enzyme matrix. We performed molecular dynamics (MD) simulations of the FAD-bound enzyme and computed the free energy changes for the electron and proton addition processes. In addition, charged residues of the surrounding enzyme matrix were studied in detail to gain insight into their role in stabilizing the charge separation that occurred as a result of the FAD reduction.

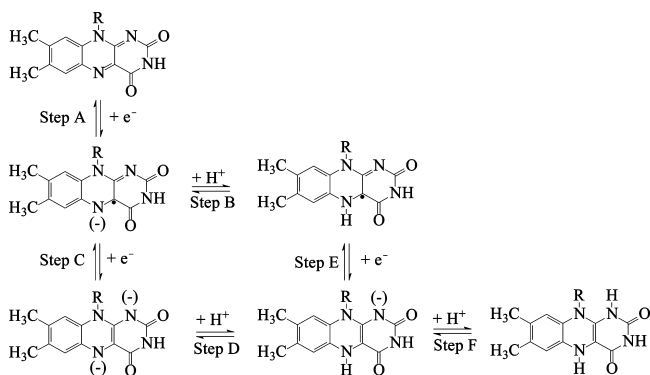
2. Computational Methods

Cartesian coordinates for the crystal structure of NQO2 enzyme (PDB code 1ZX1) were obtained from protein data bank¹⁵ and used in all computations. Visualizations and analyses of the protein structure were carried out using the Visual Molecular Dynamics¹⁶ program. All free energy calculations were performed with explicit solvent molecules using CHARMM¹⁷ program suit. Computations were carried out on an in-house server at the UWEC Chemistry Department containing nine nodes, each with eight Intel Xeon E5430 processors.

2.1. Redox and Protonation/Deprotonation Equilibria. Reduction of flavin may involve an incomplete $1e^-/1H^+$ process yielding radical semiquinones¹⁸ or a complete $2e^-/2H^+$ forming stable hydroquinone products (Scheme 1).^{19–21} Representing the NQO2-bound oxidized flavin as F, the first electron transfer

* To whom correspondence should be addressed: E-mail: bhattas@uwec.edu.

SCHEME 1



(Scheme 1) results in the formation of an unstable anionic semiquinone ($F^{\bullet-}$)



$F^{\bullet-}$ can quickly convert into the protonated neutral semiquinone form, FH^{\bullet} (Scheme 1), or may undergo another $1e^-$ reduction to form the dianionic species, F^{2-} .



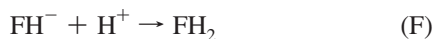
The proton transferred product of F^{2-} is obtained as anionic hydroquinone



The anionic hydroquinone can also be formed due to the reduction of neutral semiquinone radical, FH^{\bullet} , formed in step B



Finally, the anionic hydroquinone can abstract a second proton to produce neutral hydroquinone



If $\Delta G^{o(X)}(\text{aq})$ represents the Gibb's free energy change at the standard state for a process designated by X, then the net free energy change for the complete $2e^-/2H^+$ addition is obtained through summation of the quantities for the individual steps of A, C, D, and F

$$\Delta G^{o(2e^-/2H^+)}(\text{aq}) = \Delta G^{o(A)}(\text{aq}) + \Delta G^{o(C)}(\text{aq}) + \Delta G^{o(D)}(\text{aq}) + \Delta G^{o(F)}(\text{aq}) \quad (1)$$

while, the $1e^-/1H^+$ product is obtained using

$$\Delta G^{o(1e^-/1H^+)}(\text{aq}) = \Delta G^{o(A)}(\text{aq}) + \Delta G^{o(C)}(\text{aq}) + \Delta G^{o(D)}(\text{aq}) - \Delta G^{o(E)}(\text{aq}) \quad (2)$$

The standard state free energy change for step B is obtained as

$$\Delta G^{o(B)}(\text{aq}) = \Delta G^{o(1e^-/1H^+)}(\text{aq}) - \Delta G^{o(A)}(\text{aq}) \quad (3)$$

2.2. Standard Reduction Potentials and pK_a 's. Standard reduction potentials are usually expressed relative to the standard reduction potential of the normal hydrogen electrode, E_H^0 , which is 4.28 V.²² The normal hydrogen electrode is also called the standard hydrogen electrode. Therefore, the standard reduction potential of any reduction step is obtained from Gibb's free energy change, $\Delta G^o(\text{aq})$

$$E^o = -\frac{\Delta G^o(\text{aq})}{nF} - E_H^o \quad (4)$$

where n is the number of electrons involved in the reaction, F is Faraday's constant, which equals $23.06 \text{ kcal mol}^{-1} \text{ V}^{-1}$, and $\Delta G^o(\text{aq})$ is the combined free energy changes calculated using eqs 1 and 2.

The pK_a of the protonated species, XH , for steps shown in eqs B, D, and F, can be obtained readily from $\Delta G^o(\text{aq})$ of the proton addition step

$$pK_a = -\frac{\Delta G^o(\text{aq})}{2.303RT} \quad (5)$$

2.3. Thermodynamic Integration. Computations of the free energy change for the electron and proton addition steps in eqs 1 and 2 were carried out through implementation of a thermodynamic integration (TI) method.^{23,24} Briefly, in this procedure, the calculation of free energy change between two states, P and Q , is obtained using the Zwanzig formula²⁵

$$\Delta G = G_P - G_Q = -\beta^{-1} \ln \langle \exp(-\beta \Delta U) \rangle_P \quad (6)$$

where $\beta = 1/kT$ and $\langle \exp(-\beta \Delta U) \rangle_P$ represents the MD generated ensemble-averaged quantity of the potential energy difference $\Delta U = U_Q - U_P$, that is sampled using U_P potential. However, in order to obtain convergence of the ensemble averaged ΔU , the thermally accessible regions of the two potentials would need to have a significant degree of overlap, so that configurations sampled on potential U_P have a reasonable occurrence on the potential of the other state, U_Q . In practice, this is handled by defining a path between the two states using a set of intermediate hybrid potential energy functions that are constructed as linear combinations of the initial (P) and final (Q) state potentials

$$U(\theta) = (1 - \theta)U_P + \theta U_Q \quad (7)$$

where θ is the coupling parameter that is varied in small intervals from 0 to 1. Note the path chosen is arbitrary since internal energy is a state function. Separate MD simulations are carried out at each intermediate value of θ . The total free energy difference is obtained through summation of the free energy changes over all intermediate intervals.^{23,24} Following literature discussions,²⁶ the total free energy change of the process is expressed as

$$\Delta G = \int_0^1 \left\langle \frac{\partial U(\theta)}{\partial \theta} \right\rangle_{\theta} d\theta \quad (8)$$

The ensemble-averaged partial derivative of the potential energy, $\langle (\partial U(\theta))/(\partial \theta) \rangle_{\theta}$, was calculated with a specific value of θ in each simulation, from eq 7 as

$$\left\langle \frac{\partial U(\theta)}{\partial \theta} \right\rangle_{\theta} = \langle U_Q - U_P \rangle_{\theta} \quad (9)$$

where the quantity $\langle \rangle_{\theta}$ indicates that the average was calculated using multiple conformations that were sampled using the intermediate potential (eq 7) for a specific value of θ . For each configuration, the same Cartesian coordinates were used for calculating energetics of two topologies for the two states P and Q (i.e., two potential functions for P and Q). This method is referred to as a dual topology single coordinate (DTSC) scheme.^{27,28}

2.4. QM/MM Partition. In this study, we have used SCC-DFTB^{12–14} theory in conjunction with MM. The advantages for using SCC-DFTB^{12–14} is that it incorporates a self-consistent-field treatment of electron–electron interactions into tight-binding theory,²⁹ which assumes the electronic state of a molecule as a linear combination of the atomic states of all of the constituent atoms. In particular, the exchange–correlation functional derived by Perdew, Burke, and Ernzerhof³⁰ was used to calculate electron–electron correlation energy. The calculation of electron–electron interaction is thereby simplified by considering atom-centered point charges, which are calculated by Mulliken population analysis.^{12,31} Furthermore, an important feature in the SCC-DFTB model is that it has been parametrized^{13,14} to fit properties from DFT-B3LYP calculations, providing more quantitative results than the standard extended Hückel model.³² Therefore, the use of SCC-DFTB has provided accuracy in predicting biomolecular properties and energetics where electronic structure changes are significant.^{11,12,27,31,33–35}

In the present study, the dimethylisalloxazine (i.e., flavin) ring atoms of FAD constitute the primary subsystem (PS) (Scheme 2) and were described by high-level theory (vide infra) that could account for the change in the electronic structure upon redox transitions, which is an important quantum mechanical (QM) effect.³³ All of the remaining atoms are included in the secondary subsystem (SS) and were treated with MM potentials (Scheme 2). The energy of such a partitioned entire system (ES), comprised of solvent-cofactor-enzyme, can be expressed as

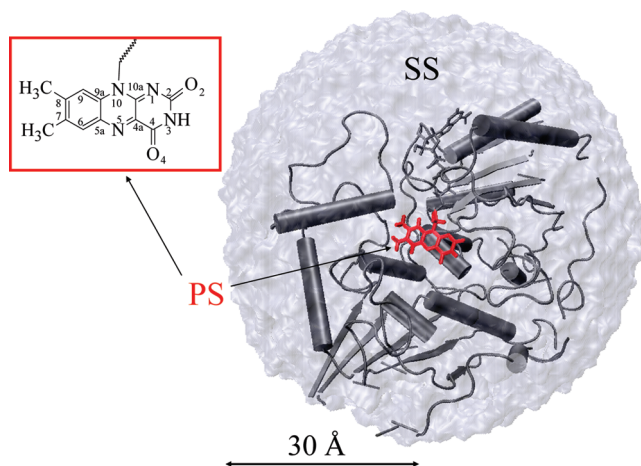
$$E_{\text{Total}}(\text{ES}) = E_{\text{QM}}(\text{PS}) + E_{\text{QM/MM}}(\text{PS/SS}) + E_{\text{MM}}(\text{SS}) \quad (10a)$$

and thus the potential energy of a specific state P takes the form of

$$U_P = \langle \Psi(P) | H_{\text{QM}}^0(P) + H_{\text{QM/MM}}(P) | \Psi(P) \rangle + U_{\text{MM}}(P) \quad (10b)$$

where $H_{\text{QM}}^0(P)$ represents the Hamiltonian operator for the PS (flavin ring atoms) in the gas-phase, Ψ_P is the converged electronic self-consistent-field wave function of the PS, $H_{\text{QM/MM}}(P)$ is the QM/MM interaction Hamiltonian operator for the PS/SS, and U_{MM} is the classical mechanical energy, obtained from the molecular mechanically described potentials of the entire SS. Simplification of eq 10b yields

SCHEME 2



$$U_P = E_g^0(P) + U_{\text{QM/MM}}(P) + U_{\text{MM}}(P) \quad (10c)$$

where $E_g^0(P)$ provides the gas-phase energy and $U_{\text{QM/MM}}(P)$ is the PS/SS interaction energy.

Following partition of the system, as described above, the flavin ring atoms were treated quantum mechanically with SCC-DFTB,^{12–14} while the remaining atoms (of cofactor, enzyme, and solvent molecules) were treated classically using CHARMM22 all-atom force fields.^{36,37} Stochastic boundary conditions³⁶ were employed to simulate enzyme solvent interactions; however, the QM/MM boundary was treated by the link atom method.³⁵

2.5. Setting up the Structure. The cofactor-enzyme-solvent complex was setup following a procedure described earlier.^{11,38} Briefly, a center was defined taking the geometric average of the flavin ring atoms. The enzyme-bound cofactor was subsequently solvated by placing the defined center into a water sphere of a radius of 30 Å. All protein atoms beyond 30 Å from this center were also deleted. Atoms within 24 Å were treated by Newtonian dynamics, while Langevin's dynamics was employed in the region 24–30 Å, where the frictional forces between the atoms were gradually increased toward the boundary.³⁸ Water molecules were treated by the three-point-charge TIP3P model.³⁹ All nonbonded interactions were truncated using a switching function between 12–14 Å, and the dielectric constant was kept at unity. The SHAKE algorithm⁴⁰ was used to constrain the bond lengths and bond angles of the hydrogen atoms. A time step of 1 fs was used in the leapfrog Verlet algorithm for integration.^{41,42} For conformation sampling, we used the canonical (NVT) ensemble, which in principle would produce Helmholtz free energy changes, but has been approximated as the Gibbs free energy in the condensed-phase reactions. Finally, in order to keep the reaction zone intact, a deformable boundary potential corresponding to a 30 Å solvent sphere⁴³ was applied to all solvent atoms in the system.

2.6. Free Energy Calculations. Following the TI method, the free energy change for a specific reaction in an aqueous solution was calculated from the plot of the ensemble-averaged partial derivative of the potential energy (with respect to the coupling parameter), $\langle (\partial U(\theta))/(\partial \theta) \rangle_{\theta}$ versus the coupling parameter, θ . The data points were fitted to a regression line and the free energy change was obtained from the integrated sum of the function over θ , which was varied from 0 to 1. However, as described in the following section, in order to compare the computed energy quantity with the experimentally observed results, the free energy changes for the electron and proton

addition processes needed additional corrections. The corrected free energy changes for both processes were obtained

$$\Delta G^{\circ}(\text{aq}) = \Delta G_{\text{uncorr}}^{\circ}(\text{aq}) + \Delta G_{\text{corr}} \quad (11)$$

where $\Delta G_{\text{uncorr}}^{\circ}(\text{aq})$ is the uncorrected standard-state free energy changes and ΔG_{corr} is the correction term. The calculations for ΔG_{corr} were carried out according to published procedure¹¹ and are given as Supporting Information. Briefly, the uncorrected free energy for both proton and electron addition was obtained from the thermodynamic integration method (Section 2.3), but were corrected for vibrational and electronic effects¹¹ and for electrostatic effects of atoms beyond 30 Å of the stochastic boundary (general Born's corrections⁴⁴). Additionally, a high-level correction was also introduced, where the SCC-DFTB computed gas-phase energies of the flavin atoms¹¹ were corrected using high-level DFT calculation with M06-L⁴⁵ functional with 6-31+G(d,p) basis set (see Supporting Information).

2.7. Charge-Neutralization Calculations. In order to quantitatively estimate the electrostatic impact of each charged residue on the free energy, we calculated the change in the electrostatic component of the PS/SS (QM/MM) interaction energy when the charge of that specific residue was abolished

$$\Delta E_{\text{elec}} = E_{\text{elec}}^0 - E_{\text{elec}}^{\delta} \quad (12a)$$

where E_{elec}^0 and E_{elec}^{δ} are the interaction energies before and after the charge on the specific residue is abolished. Therefore, the quantity obtained in ΔE_{elec} contains the net effect of the partial charges (indicated by δ) of all atoms of that specific residue on the particular redox state of the PS in the protein. Therefore, the difference of the ΔE_{elec} energies between the two redox states is a measure of the relative contribution of that charged residue in a specific redox reaction (Table 3)

$$\Delta \Delta E_{\text{elec}} = \Delta E_{\text{elec}}^{\text{Rd}} - \Delta E_{\text{elec}}^{\text{Ox}} \quad (12b)$$

3. Results and Discussion

3.1. Modeling of Electron Transfer Reactions in Condensed Phase. Electronic structure calculations have been extensively used to calculate condensed phase standard redox potentials of organic molecules, metal complexes, and electron-transfer proteins.⁴⁶ In these studies, the effect of solvation has been estimated either by continuum solvation model^{47–68} or with explicit solvent molecules.^{11,27,28,69–74} In particular, for larger and complex biomolecules, calculation of absolute redox potentials are very successful using hybrid quantum mechanical and molecular mechanical (QM/MM) methods such as SCC-DFTB^{11,27,28} and ONIOM calculation methods.^{65,66,75–78} The latter method has been used by Datta et al. in a series of calculations to determine the absolute redox potentials of a number of biomolecules^{61,65,66} while SCC-DFTB has recently been used for similar studies on various flavoenzymes.^{11,27,28}

3.2. Calculation of Free Energies. In all TI calculations, the free energy derivative of the potential expressed in eq 10b was calculated by the DTSC scheme (see the discussion in Section 2.3). If the pure states, P and Q , are represented with the wave functions Ψ_P and Ψ_Q , respectively, then the gas-phase energies of their PS can be expressed with the help of the Hamiltonians $H_{\text{QM}}^{\circ}(P)$ and $H_{\text{QM}}^{\circ}(Q)$, respectively. The interaction energies between the PS (treated by SCC-DFTB) and SS (treated

by MM) in these pure states can be obtained from their interaction Hamiltonian $H_{\text{QM/MM}}$. Therefore, the potential energy derivative in eq 9 will take the form

$$\frac{\partial U}{\partial \theta} = -\langle \Psi_P | H_{\text{QM}}^{\circ}(P) + H_{\text{QM/MM}}(P) | \Psi_P \rangle + \langle \Psi_Q | H_{\text{QM}}^{\circ}(Q) + H_{\text{QM/MM}}(Q) | \Psi_Q \rangle \quad (13)$$

the U_{MM} terms for the P and Q states cancel each other since they are calculated entirely on same atomic coordinates of the SS using identical classical potential functions. There are two important features of eq 13. First, $H_{\text{QM}}^{\circ}(P)$ being the gas-phase contribution (see eq 10c), the difference of the gas-phase energy of the two states can be corrected using higher-level theory as described in Section 2.6. Second, it can be assumed that the stretch, bend, torsion, and van der Waals parameters (i.e., the parameters of the “bonded interactions”) in the interaction Hamiltonians are independent of the change of state; thus only the electrostatic interactions contribute to eq 13. Therefore, the computed partial derivatives of the potential energy of the system contains primarily the electrostatic response of the SS toward a perturbation at the PS due to a electron/proton addition. This computational approach is expected to provide accuracy in both the reduction potential and $\text{p}K_{\text{a}}$ calculations.

In the present case, M06-L was used as high-level theory to correct the gas-phase energy. M06-L employs a new exchange-correlation functional⁴⁵ under the local density approximation of the uniform-electron-gas model to account for the electron–electron correlation. A series of calculations showed that the new functional is capable of producing accurate energetics for delocalized π -electron systems⁴⁵ including the flavin,¹¹ which is the redox center of the present study. Being dependent on a local functional, energy calculations are much faster than hybrid functionals or the advanced molecular orbital calculation such as employing Møller–Plesset second order perturbation (MP2)⁷⁹ theory.

3.3. Convergence. The ensemble average of the partial derivative of the potential energy with respect to the coupling parameter (θ), $\langle (\partial U(\theta))/(\partial \theta) \rangle_{\theta}$, was plotted against the simulation time. A representative plot of $\langle (\partial U(\theta))/(\partial \theta) \rangle_{\theta}$ plotted against the length of simulation for various values of θ is shown in Figure 1a. It appears that the convergence of $\langle (\partial U(\theta))/(\partial \theta) \rangle_{\theta}$ was obtained long before 350 ps. In order to know what amount of simulation would suffice, we calculated the absolute %RSD $\langle (\partial U(\theta))/(\partial \theta) \rangle_{\theta}$ in a time data set of 50 ps. The fluctuations of these moving %RSDs were plotted against time (ps), for various values of θ (Figure 1b), where the ordinate of each point on the curve represents the %RSD value at the time point (denoted by the abscissa) calculated from the 50 ps MD simulation data preceding this time point. It appears that the %RSD of all these $\langle (\partial U(\theta))/(\partial \theta) \rangle_{\theta}$ oscillates as it converges. The plot in Figure 1b indicates that the %RSD reaches close to 0.5 after 150 ps and after exactly 350 ps of simulation the %RSD value varies between 0.1–0.4%. This clearly illustrates the convergence of the derivatives and indicates that after this length of simulation was carried out, the intermediate potential energy functions were capable of generating enough configurations that had reasonable occurrences in both end states.

3.4. Reduction Potentials. Representative plots of $\langle (\partial U(\theta))/(\partial \theta) \rangle_{\theta}$ variations with θ for an electron addition (Scheme 1, step A) and a proton addition (Scheme 1, step D) reactions are shown in Figure 2. The linearity of these plots clearly conforms to the linear response theory,⁸⁰ which predicts the linear nature of the

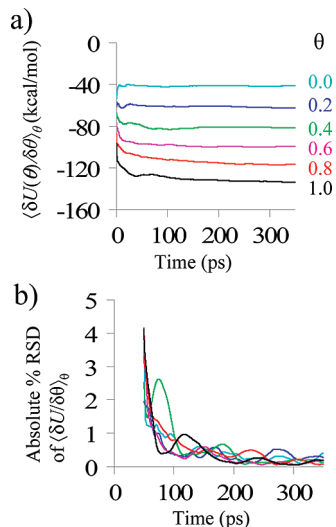


Figure 1. Convergence of the ensemble-averaged partial derivative of the potential energy with respect to the coupling parameter, $\langle \delta U(\theta) / \delta \theta \rangle_{\theta}$. (a) A representative plot of the $\langle \delta U(\theta) / \delta \theta \rangle_{\theta}$ vs simulation time (ps) is shown for the electron addition reaction $\text{FH}^{\bullet} \rightarrow \text{FH}^{-}$ and (b) the absolute % relative standard deviation (%RSD) of the $\langle \delta U(\theta) / \delta \theta \rangle_{\theta}$, calculated in 50 ps segment of the simulation data points is plotted against the simulation time (ps).

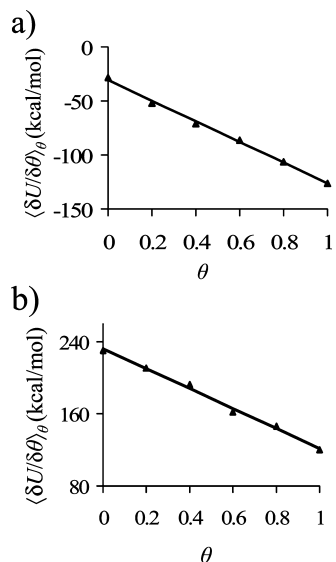


Figure 2. Representative plots for the variations of the ensemble-averaged partial derivative of the potential energy with respect to coupling parameter, $\langle \delta U(\theta) / \delta \theta \rangle_{\theta}$ obtained by thermodynamic integration calculation (a) the electron addition reaction $\text{F} \rightarrow \text{F}^{\bullet}$; (b) a proton dissociation reaction $\text{F}^{2-} \rightarrow \text{FH}^{-}$.

dielectric responses, of this enzyme active site, toward the charge separation that is caused in the redox and protonation/deprotonation processes.

It is well-known that in these flavoenzymes, the reduction processes (electron addition) are significantly coupled to proton additions.^{9,10} Therefore, the Gibbs's free energy changes for proton transfer processes were also computed in order to obtain these reduction potentials of the flavin-bound enzymatic system.

The free energy changes for the electron and proton transfer reactions (shown in Section 2.1, eqs A–F) are reported in Table 1. The free energy change due to the first electron transfer to neutral flavin (i.e., F in Scheme 1) is -90 kcal/mol, which is quite comparable to that of the second electron transfer to anionic semiquinone ($\text{F}^{\bullet-}$), which is -87 kcal/mol. However,

TABLE 1: Calculated Standard State Free Energies (kcal/mol) and Their Standard Reduction Potentials (E°), for Various NQO2-Bound Flavin States^a

reaction	$\Delta G^{\circ}(\text{aq})$ (kcal/mol)	$E^{\circ}(\text{mV})$
$\text{F} + \text{e}^{-} \rightarrow \text{F}^{\bullet-}$	-89.7	-390
$\text{F}^{\bullet-} + \text{e}^{-} \rightarrow \text{F}^{2-}$	-86.5	-529
$\text{F} + \text{e}^{-} + \text{H}^{+} \rightarrow \text{FH}^{\bullet}$	-93.9	-208 (-200) ⁸¹
$\text{FH}^{\bullet} + \text{e}^{-} + \text{H}^{+} \rightarrow \text{FH}_2$	-100.4	$+73$
$\text{F} + 2\text{e}^{-} + \text{H}^{+} \rightarrow \text{FH}^{-}$	-195.1	-50 (-159) ⁸¹

^a The values in parentheses show the experimentally determined reduction potentials for NQO1.

if a coupling of the individual electron and proton transfer reactions (eqs 1 and 2) is taken into consideration, the second coupled $1\text{e}^{-}/1\text{H}^{+}$ transfer reaction ($\Delta G^{\circ}(\text{aq}) = -100$ kcal/mol) appears considerably more favorable (by 6 kcal/mol) than that of the first $1\text{e}^{-}/1\text{H}^{+}$ transfer reaction ($\Delta G^{\circ}(\text{aq}) = -94$ kcal/mol) (Table 1). Although, this computation does not analyze if two such coupled electron–proton transfers will occur as a single-step or through a two-step process, the strong favorability of the second coupled electron–proton transfer indicates that a two-electron transferred flavin will be stabilized at the NQO2 active site after the end of the reductive half-cycle. This observation is of potential significance, since in the oxidative half-cycle, the quinone reductases are known to catalyze the transfer of two reductive equivalents to the quinones to form hydroquinone in a single step, without formation of the semiquinone.^{3,4} The prerequisite of this step is the two-electron transferred species, whose thermodynamic favorability is predicted from the present computational study.

The $1\text{e}^{-}/1\text{H}^{+}$ reduction potential calculated in this study is -200 mV, which is considerably more negative than the midpoint potential (the potential for the overall $2\text{e}^{-}/2\text{H}^{+}$ reduction of flavin) obtained for NQO2, which is -50 mV (Table 1). The experimental value of the potential of a similar enzyme (NQO1 or DT-diaphorase), whose active site bears 80% sequence homology with NQO2, is available for comparison. Using potentiometric measurements,⁸¹ this study determined a midpoint potential of -159 mV (Table 1). The estimated $1\text{e}^{-}/1\text{H}^{+}$ reduction potential from this study was -208 mV. The present theoretically determined values of the two redox potentials are thus in excellent agreement with the experimental observations (Table 1).

3.5. pK_a Calculations. The pK_a 's of the N5 proton for semiquinone (FH^{\bullet}) and N1 proton for hydroquinone (FH_2) was computed in this study (Table 2). The pK_a of semiquinone was found to be 3.0. The low pH demonstrated that the anionic semiquinone would be more stable relative to the neutral semiquinone. However, the present study does not model the kinetics and hence is unable to predict the extent of semiquinone stabilization at the NQO2 active site. Although no experimental study has reported the occurrence of anionic semiquinone of NQO2, the potentiometric study of Tedeschi et al. was able to demonstrate the transient occurrence of anionic flavosemiquinone in NQO1,⁸¹ whose active site bears a 80% sequence homology to that of NQO2. Therefore, the observed favorability of the anionic semiquinone over the neutral semiquinone is quite consistent to the experimental findings.

The pK_a of hydroquinone, FH_2 , is found to be close to 0 (Table 2), which demonstrated that the hydroquinone will certainly be deprotonated. Therefore, the present study asserts that the active site of NQO2 is capable of stabilizing the anionic hydroquinone state, FH^{-} over the neutral FH_2 . In contrast, the second pK_a of FH_2 , calculated for the N5 proton of the anionic

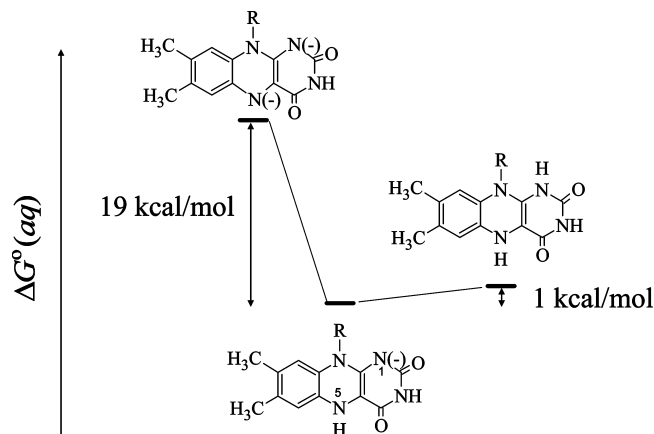


Figure 3. Stabilization of FADH^- in the NQO2 active site. R represents the ribityl-5'-ADP part of the FAD molecule.

TABLE 2: Calculated Standard State Free Energies (kcal/mol) and pK_a for Various NQO2-Bound Flavin States

reaction	flavin atom	$\Delta G^\circ(\text{aq})$ (kcal/mol)	pK_a
$\text{F}^- + \text{H}^+ \rightarrow \text{FH}^-$	N5	-4.2	3
$\text{FH}^- + \text{H}^+ \rightarrow \text{FH}_2$	N1	0.8	0
$\text{F}^{2-} + \text{H}^+ \rightarrow \text{F}^-$	N5	-18.9	14

hydroquinone is extremely high ($\text{pK}_a = 14$), indicating that a dianionic hydroquinone species would be thermodynamically quite unfavorable in the NQO2 active site.

These two results, when combined, present a picture of the active site energetics that is quite familiar to the redox chemistry of these flavoenzymes. During the catalytic reduction process, the electron is transferred as a hydride or a combination of 2 electrons and 1 proton. Therefore, the product NQO2-bound anionic flavohydroquinone (FH^-) is the hydride transferred intermediate separating reductive and oxidative half cycles. According to the present calculation, this species is the most stable one among all electron and proton transferred products. In terms of free energy difference, this hydride transferred species is stabilized by an energy of 19 kcal/mol compared to the F^{2-} and by 1 kcal/mol compared to FH_2 (Figure 3). The high pK_a of the N5 in NQO2-bound FH^- further suggests that the location of the hydride is most likely to be on N5, conforming nicely to the notion that this nitrogen atom of the isoalloxazine ring behaves as a hydride acceptor site in the enzyme catalysis.⁸²

3.6. Quantitative Analysis of the Effect of Charged Residues. The effect of individual charged residue on the PS/SS interaction energy (ΔE_{elec}) was explored using the simulation data. The quantity, ΔE_{elec} , for various charged residues within 10 Å of the PS (Figure 4) was computed using eq 12a. Computed values of the ΔE_{elec} for the NQO2-bound flavin states (i.e., neutral (F), anionic semiquinone ($\text{F}^{\bullet-}$), neutral semiquinone (FH^\bullet), and the anionic (FH^-)) for these residues are given in Table 3. A positive value indicates that the PS responded unfavorably to the annihilation of the charge of the residue. In other words, a positive ΔE_{elec} means that the individual charge of the residue induced a stabilizing effect to the ES by the quantity of ΔE_{elec} . For example, in the neutral state of the flavin, the ΔE_{elec} for Tyr155 and Gly149 were found to be 15 and 7 kcal/mol, respectively (Table 3). This shows that the charges on both these two residues contribute significantly to the stabilization of the PS. Additionally, since they are not charged residues, this further indicates strong electronic interactions between these residues and the PS. Indeed, these two residues were found to form two strong hydrogen bonds with flavin

exocyclic O2, one from the backbone amide proton of Gly149 and the other from the phenolic proton of Tyr155 (Figure 4). Additionally, the charges on Asp117 and His173 (second subunit) also contributed significantly (Table 3) in stabilizing the active site. In each case, the contribution ranges from 8–10 kcal/mol.

3.7. Response of the Active Site to the Change of Flavin Redox State. Between the two flavin redox states, there are some noticeable changes in the active site geometry as well as in the electrostatics of the active site. These electrostatic and geometric variations are shown in Figures 5 and 6, respectively. As discussed in Section 2.7, $\Delta\Delta E_{\text{elec}}$ represents the change in the electrostatic contribution of a particular residue in a redox or protonation/deprotonation process. In the present study, $\Delta\Delta E_{\text{elec}}$ of residues were computed for F^- and FH^- states relative to the neutral oxidized form, F. The plot of $\Delta\Delta E_{\text{elec}}$ for various residues vs their distances from the redox center is shown in Figure 5. Therefore, a positive value of $\Delta\Delta E_{\text{elec}}$ indicates that the electrostatic contribution increased in the specific redox state of the enzyme compared to its neutral oxidized state.

F and F^- . Analysis of the active site revealed that upon reduction, Glu193 undergoes a considerable conformational change and moves quite close to a polar residue (Asn66). A close visual analysis reveals that the glutamate occupies a position that is significantly close to the flavin moiety, which is the redox center. As indicated in Figure 6a,b, the distance between the carboxyl group of Glu193 and amide group of Asn66 decreases considerably going from the neutral to the semiquinone states of the flavin-bound NQO2 (Figure 6a). Formation of this new interaction between Asn66 and Glu193 is also reflected in the energetics. As shown in Figure 5a, the $\Delta\Delta E_{\text{elec}}$ for Glu193 is about 13 kcal/mol indicating a significant contribution of this residue in stabilizing the enzyme-bound flavosemiquinone state.

F and FH^- . The plot of $\Delta\Delta E_{\text{elec}}$ for various residues against the distance from the redox center is shown in Figure 5b. A notable decrease of the $\Delta\Delta E_{\text{elec}}$ was observed for Tyr155 in the FH^- state (Table 3, Figure 5), which predicts that Tyr155 will stabilize the oxidized neutral state, F, by 13 kcal/mol relative to the anionic hydroquinone. The error value in the parentheses is suggestive of a considerable inconsistency in the electronic environment of this part of the flavin ring in the sampled conformations. This observation insinuates that the interaction of Tyr155 with the flavin ring becomes considerably weakened in the anionic hydroquinone state. Indeed, the observed change in the geometry of the active site completely supports this view. The distance between the phenolic proton and the flavin's exocyclic O2 is increased significantly (3–4 Å) in the FH^- with a large uncertainty (~ 0.3 Å) associated with it (Figure 6b). In contrast, the phenolic proton and the flavin's exocyclic O2 forms strong hydrogen bonds (1.7 Å) in both F and F^- states (Figure 6b) with an observed uncertainty of about only 0.1 Å. Therefore, the present computational model suggests that Tyr155 will have significant influence on the enzyme catalysis, which is fully consistent with the accepted role of Tyr155 in the flavin reduction.³

The calculated $\Delta\Delta E_{\text{elec}}$ (Figure 5b) also explains the role of two negatively charged residues, Glu193 and Asp117 in stabilizing the reduced state of the NQO2-bound flavin. As illustrated in Table 3 and Figure 5, a comparison of the ΔE_{elec} shows an increase of 2 and 3 kcal/mol for Asp117 and Glu193, respectively, for the $\text{F} \rightarrow \text{FH}^-$ reaction. This observation suggests that in relative terms, electrostatic charges of these two residues

TABLE 3: Calculated Electrostatic Contributions for Selected Active Site Residues within 10 Å Radius of the Flavin-Bound NQO2^a

residue	subunit	ΔE_{elec} (kcal/mol)			
		F	F ⁻	FH ⁺	FH ⁻
Glu13	A	3.3 ± 0.2	3.7 ± 0.2	3.0 ± 0.2	3.2 ± 0.2
Gly149	A	7.3 ± 1.4	9.4 ± 1.4	12.7 ± 1.4	7.0 ± 1.9
Tyr155	A	15.3 ± 2.4	14.5 ± 2.1	16.8 ± 1.8	3.4 ± 2.8
Glu193	A	2.0 ± 0.4	9.9 ± 1.0	6.3 ± 0.6	5.1 ± 0.5
Arg200	A	-1.1 ± 0.2	-2.1 ± 0.3	-0.8 ± 0.2	-1.0 ± 0.2
Asp54	B	5.1 ± 0.2	4.7 ± 0.2	5.6 ± 0.3	5.5 ± 0.2
Asn66	B	-0.1 ± 0.3	-1.9 ± 0.6	0.9 ± 0.3	0.7 ± 0.3
Glu70	B	4.0 ± 0.2	4.1 ± 0.2	4.0 ± 0.2	3.5 ± 0.2
Lys113	B	-2.9 ± 0.7	-2.6 ± 0.9	-3.4 ± 0.8	-5.0 ± 0.7
Asp117	B	7.5 ± 0.8	6.9 ± 0.8	9.1 ± 0.9	9.7 ± 0.7
Arg118	B	-3.6 ± 0.2	-3.1 ± 0.2	-3.9 ± 0.3	-4.5 ± 0.3
His173	B	9.6 ± 0.6	9.3 ± 0.7	7.9 ± 0.5	8.1 ± 0.6
His177	B	3.5 ± 0.3	3.4 ± 0.3	2.3 ± 0.2	2.6 ± 0.2

^a The quantity ΔE_{elec} was calculated using eq 12a. F is the short-hand notation of the NQO2-bound flavin.

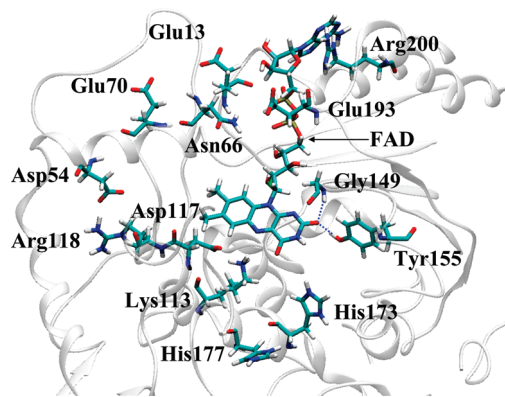


Figure 4. A 10 Å subset of the NQO2 active site surrounding the 7,8-dimethyl isoalloxazine (flavin) ring. Hydrogen bonding interactions of flavin with Gly149 and Tyr155 are indicated with blue dotted lines. The C, H, N, and O atoms are shown in cyan, white, blue, and red, respectively.

will stabilize the anionic hydroquinone state of the NQO2-bound flavin. In contrast, positively charged residues, Lys113, Arg118, and His173, have been found to stabilize the oxidized state of the flavin. This is evident from the plot of $\Delta\Delta E_{\text{elec}}$ (Figure 5b), which shows that in relative measure, the oxidized state of the flavin (F) is favored by 1–2 kcal/mol by the electrostatic interactions of these residues.

In a broader context, the electrostatic effects of charged residues observed in ΔE_{elec} reveal a familiar acid–base chemistry in the solvated enzyme active site pocket. If the solvent encapsulated FH₂ is considered as a weak acid, then the negative charge bearing residues (Brønsted bases) will favor the deprotonation of FH₂. On the other hand, positive charge-bearing residues will behave as Brønsted acids and therefore will favor the protonation of the anionic FH⁻. However, these electrostatic effects differ from a pure aqueous solution because in an enzyme active site, the polarization encompasses atoms from not only solvent molecules but also enzyme backbone and side chains amidst a hydrogen bonding network shaped by the polypeptide folding.

The polarization of the NQO2 active site, therefore, can be illustrated by the hydrogen bonding network around the flavin ring shown in Figure 7. Glu193 shown at the top interacts with a number of water molecules that are in direct contact with the flavin ring. The space between Glu193 and the flavin ring is completely filled with water. The water molecules, w1 and w2, shown in the Figure 7 are found to be within 3–4 Å of the

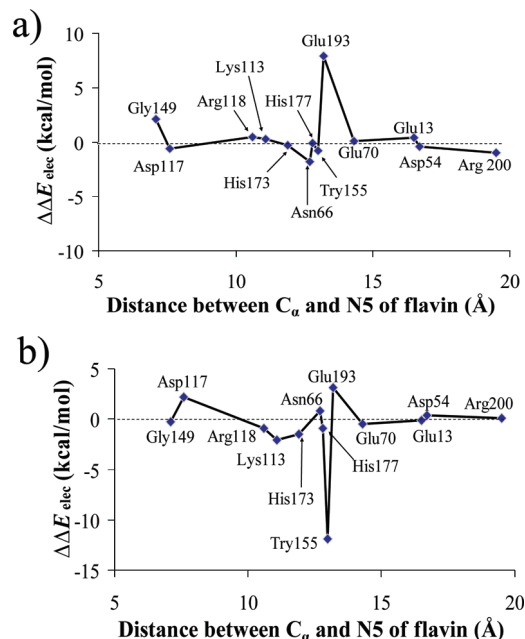


Figure 5. Comparative electrostatic stabilization energies of the individual active site residues between various NQO2 redox states. The $\Delta\Delta E_{\text{elec}}$ of various residues were plotted against the distances of their C_α atoms from the N5 atom of the flavin ring for (a) F → F⁻ and (b) F → FH⁻ reactions. These distances are calculated from the atomic coordinates of the X-ray structure of PDB code: 1ZX1.

carboxyl group of the Glu193, while w3 is within 3–5 Å of the flavin N5 atom during 50 ps dynamics. Down below the flavin ring, Asp117 forms a salt-bridge with Lys113 and the latter interacts with the flavin ring (N5) through a series of hydrogen bonds including the backbone of Trp105 and Phe106 (Figure 7). From the right-hand side, a network of hydrogen bond originating from His173 propagates through Asn161 and two other water molecules, w4 and w5, finally reaching at the flavin exocyclic atom O2. These water molecules were found to maintain the hydrogen bonding with the Asn161 and the flavin O2 throughout the 50 ps simulation.

Taken together, the observed ΔE_{elec} gives a quantitative measure of the effect of each charged active site residues on the F → FH⁻ reaction equilibrium, while the geometry analysis provides an insight into the polarization through the hydrogen bonding network in the active site that stabilizes the negative charge of the anionic hydroquinone state.

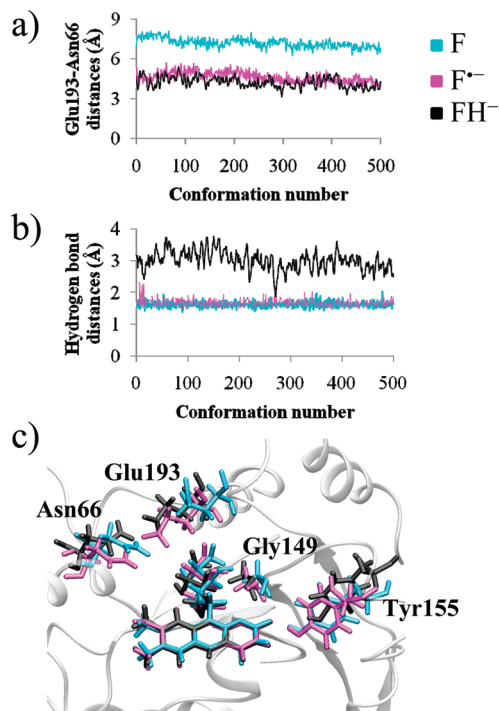


Figure 6. Geometric changes in the NQO2 active site. Fluctuations of distances calculated from the stored 500 conformations of MD simulated trajectories (a) between Glu193 (amide nitrogen) and Asn66 (carbon of the carboxylic acid) and (b) hydrogen bonding distance of the flavin exocyclic O2 with Tyr155 (proton of the phenolic hydroxyl group); (c) the superimposed active sites for F (cyan), $F^{\bullet-}$ (magenta), and FH^- (black) are shown with Gly149, Tyr155, Glu193, and Asn66 residues surrounding the tricyclic 7,8-dimethyl 10-ribityl isoalloxazine moiety of the FAD at the center.

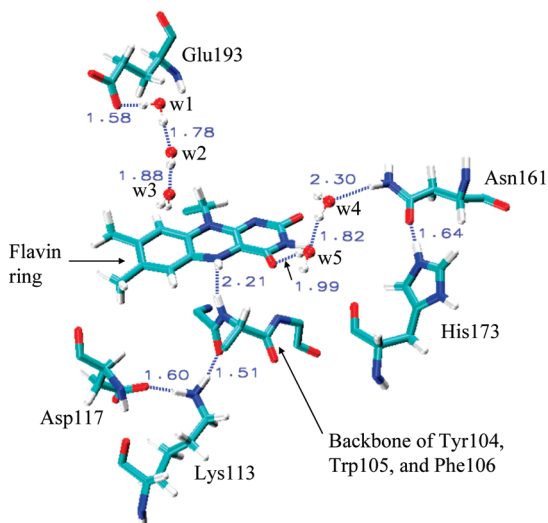


Figure 7. The hydrogen bonding interaction network of the important charged residue with the flavin is shown at the NQO2 active site. The color codes of atoms are identical to that used in Figure 4.

4. Conclusions

Using hybrid SCCDFTB/MM potentials-based molecular dynamics (MD) simulations, we have computed the redox potentials for NQO2. The free energy changes for the redox and protonation-deprotonation processes of the enzyme-bound flavin were calculated using thermodynamic integration methods. The $2e^-/2H^+$ potentials of NQO2 have been determined to be about -50 mV, which is 100 mV positive to the experimentally determined reduction potential of NQO1,^{3,81} whose flavin binding site bears 80% similarity in terms of sequence homology.

The computed redox potential of the $F \rightarrow F^{\bullet-}$ was found to be around -200 mV, which is quite close to the estimated midpoint potential (-208 mV). Analysis of the simulated data shows that the conformational change of a nonconserved glutamate residue (Glu193) is strongly linked to the stabilization for the one-electron reduction process and the charge on Glu193 contributes 8 kcal/mol for the stabilization of the anionic semiquinone.

The present study demonstrates that the complete reduction of the flavin moiety produces an anionic semiquinone, FH^- that is stabilized by the NQO2 active site environment. The pK_a of the N1 proton of the NQO2-bound FH_2 is extremely low (<1.0) indicating that the neutral hydroquinone, FH_2 would not be stabilized. The stability of FH^- is also evident from the observation of a very high pK_a (~ 14) of the flavin N5 proton that could yield the dianionic species, F^{2-} . Observation of a stable FH^- is absolutely consistent with the mediatory role of N5 in the catalytic hydride transfer reaction catalyzed by these flavoenzymes.

Subsequent analysis of the simulated data reveals that negatively charged residues, Asp117 and Glu193, contributes in stabilizing the anionic hydroquinone. The Glu193 residue is known to play a key role in the binding of dopamine, one of NQO2 substrates.⁴ The simulation has also demonstrated that Tyr155 is instrumental in destabilizing the FH^- state when compared to the neutral oxidized state.

Quinone reductases provide a classic example of a catalytic mechanism in which the binding of the substrate/cosubstrate shows selectivity of the oxidation state of the cofactor, FAD. In the present calculation, we observed that positively charged residues contribute to the stability of the oxidized state, whereas negatively charged residues stabilize the reduced state. Although the molecular basis of the active site's differential recognition of substrates is unclear, the observation of two sets of oppositely charged residues influencing the two flavin redox states is significant. It suggests that the change in the flavin redox state creates not only a major electrostatic change in the vicinity of the redox site but also effects a polarization comprising a larger part of the NQO2 active site, which could potentially influence the binding and release of alternate substrates in the oxidative and reductive half-cycles. Additionally, the involvement of multiple negatively charged residues suggests a possible dynamic nature of the proton in the proton transfer process, which is strongly coupled to the electron transfer. Similar movement of protons has been observed previously by Gunner et al. in a coupled electron-proton transfer reactions of quinones in the bacterial photosynthetic reaction center in *Rb. sphaeroides*.⁸³ The resultant conformational changes and the change in the entire protein dynamics⁸³⁻⁸⁷ could be instrumental in the shuttling of substrates. Further studies on the dynamics are needed to explore this proton and protein motion. Furthermore, simulations involving substrates could shed more light on the role of specific charged residues in coordinating the substrate binding and release as the enzyme oscillates between the two flavin redox states during "ping-pong" kinetics.

Acknowledgment. We gratefully acknowledge the computational support from the LTS, University of Wisconsin-Eau Claire. We are thankful to Professor Jiali Gao for critical reading of the manuscript. We would like to thank Dr. Sanchita Hati for helpful discussions. This work was financially supported by the Office of Research and Sponsored Programs, University of Wisconsin-Eau Claire, Eau Claire, WI.

Supporting Information Available: Calculations carried out to correct the SCC-DFTB/MM results (standard state free energy changes for the electron and proton transfer reactions) are provided. This material is available free of charge via the Internet at <http://pubs.acs.org>.

References and Notes

- (1) Radjendirane, V.; Jaiswal, A. K. *Biochem. Pharmacol.* **1999**, *58*, 597.
- (2) Vella, F.; Ferry, G.; Delagrangé, P.; Boutin, J. A. *Biochem. Pharmacol.* **2005**, *71*, 1.
- (3) Colucci, M. A.; Moody, C. J.; Couch, G. D. *Org. Biomol. Chem.* **2008**, *6*, 637.
- (4) Fu, Y.; Buryanovskyy, L.; Zhang, Z. *J. Biol. Chem.* **2008**, *283*, 23829.
- (5) Deller, S.; Macheroux, P.; Sollner, S. *Cell. Mol. Life Sci.* **2008**, *65*, 141.
- (6) AbuKhader, M.; Heap, J.; De Matteis, C.; Kellam, B.; Doughty, S. W.; Minton, N.; Paoli, M. *J. Med. Chem.* **2005**, *48*, 7714.
- (7) Bianchet, M. A.; Faig, M.; Amzel, L. M. *Methods Enzymol.* **2004**, *382*, 144.
- (8) Jamieson, D.; Wilson, K.; Pridgeon, S.; Margetts, J. P.; Edmondson, R. J.; Leung, H. Y.; Knox, R.; Boddy, A. V. *Clin. Cancer Res.* **2007**, *13*, 1584.
- (9) Cukier, R. I. *J. Phys. Chem.* **1996**, *100*, 15428.
- (10) Cukier, R. I.; Nocera, D. G. *Annu. Rev. Phys. Chem.* **1998**, *49*, 337.
- (11) Bhattacharyya, S.; Stankovich, M. T.; Truhlar, D. G.; Gao, J. *J. Phys. Chem. A* **2007**, *111*, 5729.
- (12) Cui, Q.; Elstner, M.; Kaxiras, E.; Frauenheim, T.; Karplus, M. *J. Phys. Chem. B* **2001**, *105*, 569.
- (13) Elstner, M.; Porezag, D.; Jungnickel, G.; Elstner, J.; Haugk, M.; Frauenheim, T.; Suhai, S.; Seifert, G. *Phys. Rev. B* **1998**, *58*, 7260.
- (14) Frauenheim, T.; Seifert, G.; Elstner, M.; Hajnal, Z.; Jungnickel, G.; Porezag, D.; Suhai, S.; Reholz, R. *Phys. Status Solidi B* **2000**, *217*, 41.
- (15) Berman, H. M.; Westbrook, J.; Feng, Z.; Gilliland, G.; Bhat, T. N.; Weissig, H.; Shindyalov, I. N.; Bourne, P. E. *Nucleic Acids Res.* **2000**, *28*, 235.
- (16) Humphrey, W.; Dalke, A.; Schulten, K. *J. Mol. Graphics* **1996**, *14*, 33.
- (17) Brooks, B. R.; Brucoleri, R. E.; Olafson, B. D.; States, D. J.; Swaminathan, S. *J. Comput. Chem.* **1983**, *4*, 187.
- (18) Janik, B.; Elving, P. *J. Chem. Rev.* **1968**, *68*, 295.
- (19) Ghisla, S.; Massey, V. *Eur. J. Biochem.* **1989**, *181*, 1.
- (20) Mayhew, S. G. *Eur. J. Biochem.* **1999**, *265*, 698.
- (21) Walsh, J. D.; Miller, A.-F. *J. Mol. Struct.* **2003**, *623*, 185.
- (22) Kelly, C. P.; Cramer, C. J.; Truhlar, D. G. *J. Phys. Chem. B* **2006**, *110*, 16066.
- (23) Beveridge, D. L.; Mezei, M.; Ravishanker, G.; Jayaram, B. *Proc. Int. Symp. Biomol. Struct. Interact., Suppl. J. Biosci.* **1985**, *8*, 167.
- (24) Straatsma, T. P.; Berensden, H. J. C. *J. Chem. Phys.* **1988**, *89*, 5876.
- (25) Zwanzig, R. W. *J. Phys. Chem.* **1954**, *22*, 1420.
- (26) Brandsdal, B. O.; Osterberg, F.; Almlof, M.; Feierberg, I.; Luzhkov, V. B.; Aqvist, J. *Adv. Protein Chem.* **2003**, *66*, 123.
- (27) Formanek, M. S.; Li, G.; Zhang, X.; Cui, Q. *J. Theor. Comp. Chem.* **2002**, *1*, 53.
- (28) Li, G.; Zhang, X.; Cui, Q. *J. Phys. Chem. B* **2003**, *107*, 8643.
- (29) Slater, J. C.; Koster, G. F. *Phys. Rev.* **1954**, *94*, 1498.
- (30) Perdew, J. P.; Burke, K.; Ernzerhof, M. *Phys. Rev. Lett.* **1996**, *77*, 3865.
- (31) Elstner, M.; Cui, Q.; Munih, P.; Kaxiras, E.; Frauenheim, T.; Karplus, M. *J. Comput. Chem.* **2003**, *24*, 565.
- (32) Zerner, M. C. *Rev. Comp. Chem.* **1991**, *8*, 313.
- (33) Liu, H.; Elstner, M.; Kaxiras, E.; Frauenheim, T.; Hermans, J.; Yang, W. *Proteins* **2001**, *44*, 484.
- (34) König, P. H.; Hoffmann, M.; Frauenheim, T.; Cui, Q. *J. Phys. Chem. B* **2005**, *109*, 9082.
- (35) Woodcock, H. L.; Hodosek, M.; Brooks, B. R. *J. Phys. Chem. A* **2007**, *111*, 5720.
- (36) Pavelites, J. J.; Gao, J.; Bash, P. A.; MacKerell, A. D. *J. Comput. Chem.* **1997**, *18*, 221.
- (37) MacKerell, A. D. J.; Bashford, D.; Bellott, M.; Dunbrack, R. L. J.; Evanseck, J. D.; Field, M. J.; Fischer, S.; Gao, J.; Gou, J.; Ha, S.; Joseph-McCarthy, D.; Kuchnir, L.; Kuczera, K.; Lau, F. T. K.; Mattos, C.; Michnick, S.; Ngo, T.; Nguyen, D. T.; Prodhom, B.; Reiher, W. E. I.; Roux, B.; Schelenkrich, M.; Smith, J. C.; Stote, R.; Straub, J.; Watanabe, M.; Wiórkiewicz-Kuczera, J.; Yin, D.; Karplus, M. *J. Phys. Chem. B* **1998**, *102*, 3586.
- (38) Bhattacharyya, S.; Ma, S.; Stankovich, M. T.; Truhlar, D. G.; Gao, J. *Biochemistry* **2005**, *44*, 16549.
- (39) Jorgensen, W. L.; Chandrasekhar, J.; Madura, J. D.; Impey, R. W.; Klein, M. L. *J. Chem. Phys.* **1983**, *79*, 926.
- (40) Rychaert, J. P.; Ciotti, G.; Berensden, H. J. C. *J. Comput. Phys.* **1977**, *23*, 327.
- (41) Verlet, L. *Phys. Rev.* **1967**, *159*, 98.
- (42) Hockney, R. W. *Methods Comput. Phys.* **1970**, *9*, 136.
- (43) Brooks, C. L. I.; Karplus, M. *J. Chem. Phys.* **1983**, *79*, 6312.
- (44) Born, M. *Z. Phys.* **1920**, *1*, 45.
- (45) Zhao, Y.; Truhlar, D. G. *J. Chem. Phys.* **2006**, *125*, 194101.
- (46) Lewis, A.; Bumpus, J. A.; Truhlar, D. G.; Cramer, C. J. *J. Chem. Educ.* **2004**, *81*, 596.
- (47) Reynolds, C. A.; King, P. M.; Richard, W. G. *J. Chem. Soc., Chem. Commun.* **1988**, 1434.
- (48) Gunner, M. R.; Honig, B. *Proc. Natl. Acad. Sci. U.S.A.* **1991**, *88*, 9151.
- (49) Reynolds, C. A. *Int. J. Quantum Chem.* **1995**, *56*, 677.
- (50) Boesch, S. E.; Grafton, A. K.; Wheeler, R. A. *J. Phys. Chem.* **1996**, *100*, 10083.
- (51) Raymond, K. S.; Grafton, A. K.; Wheeler, R. A. *J. Phys. Chem. B* **1997**, *101*, 623.
- (52) Olsson, M. H.; Ryde, U. *J. Biol. Inorg. Chem.* **1999**, *4*, 654.
- (53) Winget, P.; Weber, E. J.; Cramer, C. J.; Truhlar, D. G. *Phys. Chem. Chem. Phys.* **2000**, *2*, 1231.
- (54) Patterson, E. V.; Cramer, C. J.; Truhlar, D. G. *J. Am. Chem. Soc.* **2001**, *123*, 2025.
- (55) Olsson, M. H.; Ryde, U. *J. Am. Chem. Soc.* **2001**, *123*, 7866.
- (56) Fontanesi, C.; Benassi, R.; Giovanardi, R.; Marcaccio, M.; Paolucci, F.; Roffia, S. *J. Mol. Struct.* **2002**, *612*, 277.
- (57) Baik, M. H.; Friesner, R. A. *J. Phys. Chem. A* **2002**, *106*, 7407.
- (58) Namazian, M.; Norouzi, P.; Ranjbar, R. *J. Mol. Struct.* **2003**, *625*, 235.
- (59) Winget, P.; Cramer, C. J.; Truhlar, D. G. *Theor. Chem. Acc.* **2004**, *112*, 2025.
- (60) Namazian, M.; Almodarresieh, H. A. *J. Mol. Struct.* **2004**, *686*, 97.
- (61) Datta, S. N.; Sudhamsu, J.; Pandey, A. *J. Phys. Chem. B* **2004**, *108*, 8007.
- (62) Dutton, A. S.; Fukuto, J. M.; Houk, K. N. *Inorg. Chem.* **2005**, *44*, 4024.
- (63) Shamshipur, M.; Alizadeh, K.; Arshadi, S. *J. Mol. Struct.* **2006**, *758*, 71.
- (64) Jaque, P.; Cramer, C. J.; Truhlar, D. G. *J. Phys. Chem. C* **2007**, *111*, 5783.
- (65) Mehta, N.; Datta, S. N. *J. Phys. Chem. B* **2007**, *111*, 7210.
- (66) Pandey, A.; Datta, S. N. *J. Phys. Chem. B* **2005**, *109*, 9066.
- (67) Lynden-Bell, R. M. *J. Phys. Chem. B* **2007**, *111*, 10800.
- (68) Takahashi, R.; Hasegawa, K.; Noguchi, T. *Biochemistry* **2008**, *47*, 6289.
- (69) Churg, A. K.; Warshel, A. *Biochemistry* **1986**, *25*, 1675.
- (70) Shenoy, V. S.; Ichiye, T. *Proteins* **1993**, *17*, 152.
- (71) Ichiye, T. In *Computational Biochemistry and Biophysics*; Becker, O. M., MacKerell, A. D. J., Roux, B., Watanabe, M., Eds.; Dekker: New York, 2001; p 393.
- (72) Tavernelli, I.; Vuilleumier, R.; Sprik, M. *Phys. Rev. Lett.* **2002**, *88*, 213002.
- (73) Olsson, M. H.; Hong, G.; Warshel, A. *J. Am. Chem. Soc.* **2003**, *125*, 5025.
- (74) Blumberger, J.; Sprik, M. *Theor. Chem. Acc.* **2006**, *115*, 113.
- (75) Svenson, M.; Humbel, S.; Froese, R. D. J.; Matsubara, T.; Sieber, S.; Sieber, K.; Morokuma, K. *J. Phys. Chem.* **1996**, *190*, 19357.
- (76) Torrent, M.; Vreven, T.; Musaev, D. G.; Morokuma, K.; Farkas, O.; Schlegel, H. B. *J. Am. Chem. Soc.* **2002**, *124*, 192.
- (77) Prabhakar, R.; Vreven, T.; Frisch, M. J.; Morokuma, K.; Musaev, D. G. *J. Phys. Chem. B* **2006**, *110*, 13608.
- (78) Lundberg, M.; Morokuma, K. *J. Phys. Chem. B* **2007**, *111*, 9380.
- (79) Moller, C.; Plessset, M. S. *Phys. Rev.* **1934**, *46*, 618.
- (80) Simonson, T. *Proc. Natl. Acad. Sci. U.S.A.* **2002**, *99*, 6544.
- (81) Tedeschi, G.; Chen, S.; Massey, V. *J. Biol. Chem.* **1995**, *270*, 1198.
- (82) Massey, V. *FASEB. J.* **1995**, *9*, 473.
- (83) Alexov, E. G.; Gunner, M. R. *Biochemistry* **1999**, *38*, 8253.
- (84) Alexov, E. G.; Gunner, M. R. *Biophys. J.* **1997**, *72*, 2075.
- (85) Gunner, M. R.; Saleh, M. A.; Cross, E.; ud-Doula, A.; Wise, M. *Biophys. J.* **2000**, *78*, 1126.
- (86) Song, Y.; Mao, J.; Gunner, M. R. *Biochemistry* **2003**, *42*, 9875.
- (87) Zhu, Z.; Gunner, M. R. *Biochemistry* **2005**, *44*, 82.